A PRIORI INVESTIGATIONS INTO THE CONSTRUCTION AND THE PERFORMANCE OF AN EXPLICIT ALGEBRAIC SUBGRID-SCALE STRESS MODEL

A. K. Gnanasundaram, T. Pestana and S. Hickel
Faculty of Aerospace Engineering
Delft University of Technology
Kluyverweg 1, 2629HS Delft, The Netherlands
s.hickel@tudelft.nl

ABSTRACT

We investigate the underlying assumptions of Explicit Algebraic Subgrid-Scale Models (EASSMs) for Large-Eddy Simulations (LESs) through an *a priori* analysis using data from Direct Numerical Simulations (DNSs) of homogeneous isotropic and homogeneous rotating turbulence. We focus on the performance of three models: the dynamic Smagorinsky (DSM) and the standard and dynamic explicit algebraic models as in Marstorp *et al.* (2009), here refereed to as SEA and DEA. By comparing correlation coefficients, we show that the subgrid scale (SGS) stress tensor is better captured by the EA models. Overall, the DEA leads to the best performance, which is evidenced by comparing how each model reproduces the probability density function (p.d.f.) of the SGS kinetic energy production. Next, we evaluate the approximations that are inherent to EA models such as the model for the pressure-strain correlation. We analyze the performance of three pressure-strain models commonly employed in the RANS framework: the LRR-QI, the LRR-IP, and the SSG models. Again, through correlation coefficients, and by splitting the pressure contributions into slow and rapid, we assess the relative performance of each model. Finally, we test the local equilibrium assumption of Marstorp *et al.* (2009), which considers a local balance between the SGS kinetic energy production and the dissipation. The probability density function shows that the ratio of SGS kinetic energy production to dissipation is distributed over a broad range of values and that the local equilibrium assumption can be only viewed as a mathematical simplification.

INTRODUCTION

Choosing the right subgrid-scale (SGS) turbulence model for Large-Eddy Simulations (LES) is not a trivial task. On one hand, simpler mathematical models are preferred as these tend to be computationally efficient and easier to implement. On the other hand, sophisticated models might be able to capture the complex physics of turbulent flows on coarser meshes. Recently, Explicit Algebraic (EA) Subgrid-scale stress models (EASSMs) has appeared as a promising class of models for LESs. In general, EASSMs constitute a framework from which various LES models can be derived, from simple linear to more complex non-linear ones, such as the anisotropy resolving EA models of Marstorp *et al.* (2009). Similarly to other LES models, EASSMs are based on bridging concepts that were initially proposed in the context of Reynolds-Averaged Navier-Stokes (RANS). Although these concepts are not always translatable to LESs, they are still assumed to hold and are used to derive new models. Therefore, the question of whether these assumptions remain valid within the context of LESs arises.

The starting point for the derivation of EASSMs is the evolution equation for the subgrid-scale (SGS) stress tensor. Apart from the material derivative of the SGS stress tensor, this equation involves 4 other terms: turbulence transport, turbulence production, pressure-strain correlation and dissipation. The basic idea is to simplify the non-closed terms and eventually find an algebraic expression for the SGS stress tensor. To this end, the first step is the weak equilibrium assumption proposed by Rodi (1972) within the context of RANS. This removes the temporal evolution of the subgrid stress tensor and allow us to transform the previous evolution equation into an algebraic equation. Then, the substitution of a model for the pressure-strain correlation and the dissipation leads to an implicit and non-linear relation for the SGS stress tensor.

Following the steps outlined above, Marstorp *et al.* (2009) formulated EASSMs for LES. In their derivation, a modified version of the linear LRR-QI model of (Launder *et al.*, 1975) is used to replace the pressure-strain term. To avoid the non-linearity in the final expression for the SGS stress tensor, Marstorp *et al.* (2009) invoked the local equilibrium assumption, which considers that the SGS energy production $\mathcal{P}$ equals the SGS dissipation ε everywhere in the domain. Two variations of the model were proposed: a dynamic and a non-dynamic. While from the standpoint of model simplicity and computational efficiency, the modeling strategy considered by Marstorp *et al.* (2009) is well-grounded, the validity of the local equilibrium assumption remains unverified even for canonical cases of homogeneous turbulence. As for the modeling of the pressure-strain term, the need for non-linear representation has been subject of research in RANS, see Townsend (1954), Lumley (1979) and Speziale *et al.* (1992). in LES, however, similar investigations have not yet been performed. A typical approach to understand the potential and limitations of LES models consists of examining the validity of their underlying assumptions with the help of Direct Numerical Simulations (DNS).

In this study, we use DNS data from homogeneous

isotropic and rotating turbulence to an *a priori* study. First we show comparisons of EASSMs with the dynamic Smagorinsky model (DSM) and then, we investigate two important building blocks of the models: (i) the modeling of the pressure-strain term in the SGS stress evolution equation, and (ii) the assumption that the SGS kinetic energy production and dissipation are in local balance, i.e., $\mathcal{P}/\varepsilon = 1$. Statistical tools such as correlation coefficients are used to asses the overall performance of the models and the success of the linear and the non-linear pressure strain models. To bring attention to the variability of $\mathcal{P}/\varepsilon$, probability density functions (p.d.f.) are employed.

METHODOLOGY

The starting point is the DNS data for 3 homogeneous flow cases, which are obtained by solving the incompressible Navier-Stokes equations in a triple-periodic cube of sides $\mathcal{L} = 2\pi$:

$$\nabla \cdot \vec{u} = 0 \tag{1}$$

$$\frac{\partial \vec{u}}{\partial t} + \vec{u} \cdot \nabla \vec{u} + 2\vec{\beta} \times \vec{u} = -\nabla p + \nu \nabla^2 \vec{u} + \vec{f}. \tag{2}$$

Here $\vec{u}$ represents the velocity field, p is the pressure to which density has been incorporated and ν is the kinematic viscosity of the fluid. The term $\vec{f}$ on the right-hand-side (r.h.s.) of Eq. (2) is an external force that drives the flow and follows from Alvelius (1999). Its spectrum is Gaussian and is centered around the forcing wave number k_f such that $k_f/k_0 = 4$, where k_0 is the lowest wave number. The governing equations are solved by a dealised pseudo-spectral method (3/2-rule) with aid of fast Fourier transforms (Pekurovsky (2012)). Time integration is achieved by a low-storage third-order Runge-Kutta scheme in combination with the integrating factor technique of Rogallo (1977). Starting from a zero-velocity field, Eq. (2) is integrated in time until a steady-state is reached, during which flow statistics are collected. More details about the numerical simulations can be found in Pestana & Hickel (2019). The isotropic flow is characterized by a Taylor micro-scale Reynolds number $Re_\lambda = u'\lambda/\nu \approx 230$, where u' is the r.m.s. velocity and λ is the Taylor micro-scale. They serve here as a reference in the *a priori* analysis and as initial condition for the runs with rotation.

For the two additional homogeneous rotating turbulence runs, we restart the isotropic simulations and impose a system rotation $\vec{\beta}$ aligned with the 3rd direction, i.e., $\vec{\beta} = (0,0,\beta)$, where β is the rate of rotation. This requires us to solve the governing equations in a rotating frame of reference by accounting for the Coriolis force $2\vec{\beta} \times \vec{u}$ in Eq. (2). The runs with rotation are characterized by an initial micro-scale Rossby number $Ro = u'/(2\lambda\beta)$ equal 0.6 and 0.45 and are hereafter referred to as weak and strong rotation, respectively. They constitute an example of an anisotropic flow, due to the modified dynamics rendered by rotation.

In all runs, the number of degrees of freedom is $N_p = 512^3$. As reference, in the isotropic case, the resolution is $k_{max}\eta \approx 1.5$, where k_{max} is the maximum resolved wave number and η is the Kolmogorov length scale. From these results, we arbitrarily selected velocity fields in the statistical steady-state (isotropic run) or quasi steady-state (runs with rotation) for the *a priori* analysis. To correctly rep-

resent single products, the velocity fields were first evaluated on a grid with $2N_p = 1024^3$ points. Thus, all gradients required for the *a priori* study were computed in spectral space and products were evaluated in physical space like in the pseudo-spectral method.

Definitions for the a priori analysis

The *a priori* analysis starts with filtering the DNS velocity fields to obtain the filtered velocities $\widetilde{u}_i = u_i - u'_i$. Hereafter, the subscript indices denote vectorial and tensorial components, summation over repeated indices is assumed and $\widetilde{[\cdot]}$ and $[\cdot]'$ represent the filtered and the residual quantities, respectively. The filter is an isotropic box-filter with cut-off wave number $k_c/k_0 = \pi/\Delta = 16$, where Δ is the cell width in physical space. With the filtered velocities at hand, the SGS stress tensor $\tau_{ij} = \widetilde{u_i u_j} - \widetilde{u}_i \widetilde{u}_j$ is constructed. The SGS stress tensor can be further decomposed in its spherical and deviatoric part as $\tau_{ij}^s = (2k_{sgs}/3)\delta_{ij}$ and $\tau_{ij}^d = \tau_{ij} - \tau_{ij}^s$, respectively, where $k_{sgs} = \tau_{ii}/2$ is the SGS kinetic energy and δ_{ij} is the Kronecker delta. We consider three LES models: the dynamic Smagorinsky (DSM) and the two EA models as introduced in Marstorp *et al.* (2009). We refer to the EA models of Marstorp *et al.* (2009) as the standard explicit algebraic model (SEA) and the dynamic explicit algebraic model (DEA). In the following, we detail how each of these models define τ_{ij}.

The DSM approximates the deviatoric SGS stress tensor as $\tau_{ij}^d = C_S\Delta^2(\widetilde{S}_{ij}\widetilde{S}_{ij})^{1/2}$, where the constant C_S is determined dynamically as proposed by Lilly (1992) and $\widetilde{S}_{ij} = (\widetilde{u}_{i,j} + \widetilde{u}_{j,i})/2$ is the strain rate tensor. The SEA and the DEA are based on a tensorial basis expansions (Pope (1975)), i.e., $\tau_{ij} = \tau_{ij}^s + \sum_{k=1,10} G^{(k)} T_{ij}^k$, where T_{ij}^k are 10 linearly independent tensors formed from $\widetilde{S}_{ij}$ and the rotation rate tensor $\widetilde{\Omega}_{ij} = (\widetilde{u}_{i,j} - \widetilde{u}_{j,i})/2$. The functional coefficients $G^{(k)}$ depend on the invariants of $\widetilde{S}_{ij}$ and $\widetilde{\Omega}_{ij}$, and are determined through an additional relation for τ_{ij}. This supplementary equation for τ_{ij} is obtained from the time evolution equation of τ_{ij}, which is first simplified by the weak-equilibrium assumption (Rodi, 1972) to yield

$$\frac{\tau_{ij}}{k_{sgs}}(\mathcal{P} - \varepsilon) = \mathcal{P}_{ij} + \Pi_{ij} - \varepsilon_{ij}. \tag{3}$$

In Eq. (3), $\mathcal{P}_{ij}$ is the production tensor, Π_{ij} is the pressure-strain tensor, ε_{ij} is the dissipation tensor and $\mathcal{P}$ and ε are half of the trace of $\mathcal{P}_{ij}$ and ε_{ij}. Among all these terms, only $\mathcal{P}_{ij}$ is in a closed form. Hence, models must be provided for Π_{ij}, ε_{ij} and k_{sgs}. Marstorp *et al.* (2009) take the dissipation tensor as isotropic, i.e., $\varepsilon_{ij} = (2\varepsilon/3)\delta_{ij}$, and Π_{ij}, inspired by RANS, is modeled with the LRR-QI of Launder *et al.* (1975), but slightly modified:

$$\Pi_{ij}^{LRR-QI} = -C_R\varepsilon a_{ij} + C_1 k_{sgs}\widetilde{S}_{ij}$$
$$+ \frac{3}{11}(2 + 3C_2)k_{sgs}\left(\widetilde{S}_{ik}a_{kj} + a_{ik}\widetilde{S}_{kj} - \frac{2}{3}\widetilde{S}_{kl}a_{kl}\delta_{ij}\right)$$
$$+ \frac{1}{11}(10 - 7C_2)k_{sgs}\left(\widetilde{\Omega}_{ik}a_{kj} - a_{ik}\widetilde{\Omega}_{kj}\right), \tag{4}$$

where $a_{ij} = \tau_{ij}^d/k_{sgs}$ is the normalized SGS stress tensor anisotropy. The modification in Eq. (4) with respect to the original LRR-QI model, stems from the constant C_1, which

Table 1: Correlation coefficients for $\mathcal{P}$ and k_{sgs} with the DSM, the SEA and the DEA models for the three canonical homogeneous cases of turbulence: isotropic, weak rotation and strong rotation.

Model	Production ($\mathcal{P}$)			Sub-grid kinetic energy (k_{sgs})		
	iso	weak	strong	iso	weak	strong
Dynamic Smagorinsky (DSM)	0.780	0.653	0.322	-	-	-
Non-dynamic EASSM (SEA)	0.640	0.490	0.196	0.367	0.429	0.380
Dynamic EASSM (DEA)	0.770	0.647	0.310	0.599	0.685	0.613

is taken as 3/5 instead of 4/5. The other constants are $C_R = 1.5$, $C_2 = 0.4$. Next, Marstorp *et al.* (2009) consider only the first two tensors in the T_{ij}^k basis, i.e., $T_{ij}^1 = \widetilde{S}_{ij}$ and $T_{ij}^2 = \widetilde{S}_{ik}\widetilde{\Omega}_{kj} - \widetilde{\Omega}_{ik}\widetilde{S}_{kj}$. The functional coefficients $G^{(1)}$ and $G^{(2)}$ are then determined by inserting the tensorial expansion of τ_{ij} into Eq. (3), and by invoking the perfect equilibrium assumption, i.e., $\mathcal{P} = \varepsilon$, which removes the inherent non-linearity of Eq. (3) due to the product of τ_{ij} and $\mathcal{P}$ in the left-hand-side. The resulting explicit algebraic expression for τ_{ij}, for both SEA and DEA, is

$$\tau_{ij} = \frac{2}{3}k_{sgs}\delta_{ij} + \frac{k_{sgs}^2}{\varepsilon}G^{(1)}\widetilde{S}_{ij} + \frac{k_{sgs}^3}{\varepsilon^2}G^{(2)}\left(\widetilde{S}_{ik}\widetilde{\Omega}_{kj} - \widetilde{\Omega}_{ik}\widetilde{S}_{kj}\right). \quad (5)$$

To complete the model, however, equations for k_{sgs} and ε must still be supplied. Marstorp *et al.* (2009) proposed solving for $\tau^* = k_{sgs}/\varepsilon$ instead of solving for ε directly. The SEA and the DEA differ on the way k_{sgs} and τ^* are determined. While both models define a velocity scale based on Δ and $\widetilde{S}_{ij}$, the DEA involves a constant of proportionality that is determined dynamically. This affects the definitions of $G^{(1)}$ and $G^{(2)}$, which are not shown but readily found in Marstorp *et al.* (2009).

As we have seen above, a crucial step that shapes the final form of τ_{ij} is the model for Π_{ij}. Therefore, we also asses the performance of three RANS pressure-strain models in the framework of LES: the two linear models of Launder *et al.* (1975), i.e., LRR-QI (Eq. (4) with $C_1 = 3/5$) and LRR-IP, and the non-linear SSG model (Speziale *et al.* (1991)):

$$\Pi_{ij}^{LRR-IP} = -C_R\varepsilon a_{ij} + \frac{4}{3}C_2 k_{sgs}\widetilde{S}_{ij}$$
$$+ C_2 k_{sgs}\left(\widetilde{S}_{ik}a_{kj} + a_{ik}\widetilde{S}_{kj} - \frac{2}{3}\widetilde{S}_{kl}a_{lk}\delta_{ij}\right)$$
$$+ C_2 k_{sgs}\left(\widetilde{\Omega}_{ik}a_{kj} - a_{ik}\widetilde{\Omega}_{kj}\right), \quad (6)$$

where $C_R = 1.5$ and $C_2 = 0.6$, and

$$\Pi_{ij}^{SSG} = -(C_1\varepsilon + C_1^*\mathcal{P})a_{ij} + C_2\varepsilon\left(a_{ik}a_{kj} - \frac{1}{3}a_{mn}a_{nm}\delta_{ij}\right)$$
$$+ (C_3 - C_3^* II_a^{1/2})k_{sgs}\widetilde{S}_{ij} + C_4 k_{sgs}\left(\widetilde{S}_{ik}a_{kj} + a_{ik}\widetilde{S}_{kj} - \frac{2}{3}\widetilde{S}_{kl}a_{lk}\delta_{ij}\right)$$
$$+ C_5 k_{sgs}\left(\widetilde{\Omega}_{ik}a_{kj} - a_{ik}\widetilde{\Omega}_{kj}\right). \quad (7)$$

where $C_1 = 1.7$, $C_1^* = 0.9$, $C_2 = 1.05$, $C_3 = 0.8$, $C_3^* = 0.65$, $C_4 = 0.625$ and $C_5 = 0.2$. All three models are built by combining assumptions for the different parts of the pressure field, i.e., the slow part p^{slow} and the rapid part p^{rapid},

which contribute differently to the pressure-strain term. For instance, in Eqs. (4) and (6), $-C_r\varepsilon a_{ij}$ constitutes a model for the slow contribution, whereas the remaining terms model the rapid part. In Eq. (7), the slow part is modeled by $-(C_1\varepsilon + C_1^*\mathcal{P})a_{ij}$. To evaluate the modeling of each part individually, we decompose the pressure into $p = p^{rapid} + p^{slow}$, which are determined by splitting and solving the Poisson equation:

$$\frac{\partial^2 p}{\partial x_i^2} = \underbrace{-\frac{\partial \widetilde{u}_i\widetilde{u}_j}{\partial x_i\partial x_j} - \frac{\partial \widetilde{u}_i u_j'}{\partial x_i\partial x_j} + \frac{\partial u_i'\widetilde{u}_j}{\partial x_i\partial x_j}}_{Rapid} \underbrace{- \frac{\partial u_i' u_j'}{\partial x_i\partial x_j}}_{Slow}. \quad (8)$$

Then, we use p^{rapid} and p^{slow} in the definition of Π_{ij} to obtain Π_{ij}^{slow} and Π_{ij}^{rapid}. These are later compared to their respective models in Eqs. (4), (6) and (7).

CORRELATIONS FOR THE SUBGRID-SCALE STRESS TENSOR

A common way to *a priori* compare different LES models is to look at the correlation between the modeled and the actual SGS stress tensor obtained from DNS. Nevertheless, because in incompressible flows the spherical part of the SGS stress tensor can be absorbed into the pressure term, it is sufficient to contrast its deviatoric part only, i.e., τ_{ij}^d. In Fig. 1, we show the correlation between the actual and the modeled τ_{ij}^d for the DSM, the SEA and the DEA.

By comparing the isotropic case in Figs. 1a and 1b, we observe that the DSM and the SEA yield a correlation coefficient of about 0.3 for all components of τ_{ij}^d. The correlation increases further to roughly 0.5 when the DEA is considered in Fig. 1c. We also see a higher correlation level for the diagonal components of τ_{ij}^d. When rotation is considered, however, correlations are lower than from the isotropic case. In this scenario, the DSM delivers the poorest performance, and the correlation levels continue to drop with increasing rotation. In fact, the case with strong rotation is rather challenging, as the scales of motion influenced by rotation include the subgrid-scales, i.e. $\kappa_\Omega > \kappa_c$, where κ_Ω is the wave number of Zeman (1994). The effects of rotation are more pronounced in τ_{12}^d, for which the correlation coefficient drops to around 0.2, see Figs. 1b and 1c. On the other hand, in the case of SEA and the DEA, for both weak and strong rotation, the τ_{33}^d component shows a higher correlation coefficient than in the non-rotating case. We attribute this to the fact that rotation acts to destroy the velocity gradients in the direction parallel to the rotation axis, which can ultimately lead to a loss of dependency of
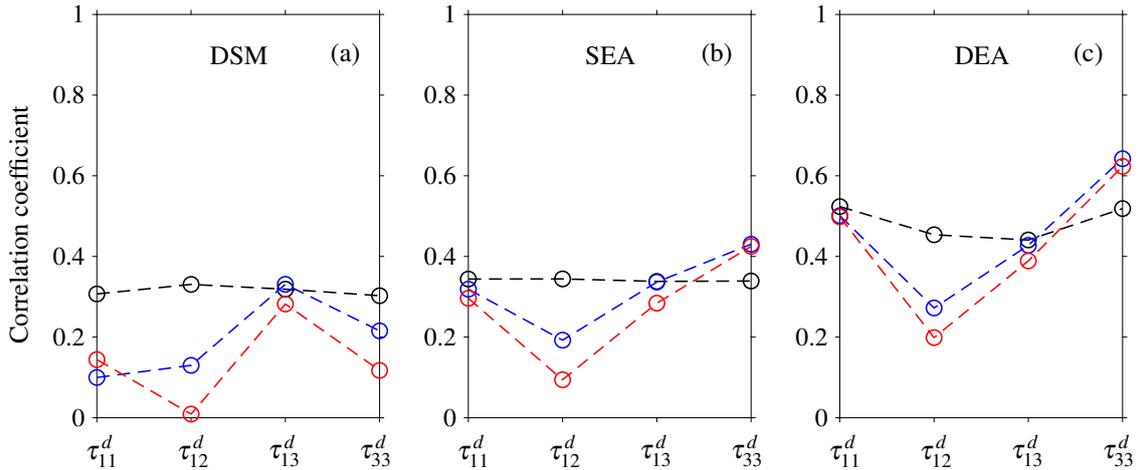
Figure 1: Correlation coefficients for the normal and cross terms of the modeled and the actual deviatoric part of the SGS stress tensor. Isotropic (-⊖-); weak rotation (-⊖-); strong rotation (-⊖-).

the flow in this direction. Thus, the same filter width can resolve a larger portion of the scales of motion in the direction of rotation in comparison with the other directions. This however, is not observed for the DSM, and the correlation of all components deteriorates in the presence of rotation.

CENTRAL ORDER MOMENTS OF SGS KINETIC ENERGY PRODUCTION

Now let us turn to the modeling of $\mathcal{P}$, which controls the amount of energy that is drained from the resolved scales, and therefore acts as a source term for k_{sgs}.

The differences between the DSM, the SEA and the DEA in modeling $\mathcal{P}$ comes from the prefactor of the strain rate tensor in the model definition. Because $\mathcal{P} = -\tau_{ij}\widetilde{S}_{ij}$, the SGS kinetic energy production depends directly on the eddy viscosity for the DSM and on $G^{(1)}k_{sgs}^2/\varepsilon$ in the case of the SEA and DEA. Although two tensors are used to construct the EA models (see Eq. (5)), only T_{ij}^1 contributes to $\mathcal{P}$, because the inner product of T_{ij}^2 and $\widetilde{S}_{ij}$ is zero.

We find that, for the isotropic case, the correlation coefficient for $\mathcal{P}$ is above 0.75 for both dynamic models, see Tab. 1. In contrast, the SEA delivers with 0.64 the lowest correlation coefficient. This discrepancy between the SEA and the DEA can be attributed to the poor modeling of k_{sgs}, as also seen in Tab. 1. Note that k_{sgs} is not modeled by the DSM and therefore not listed in Tab. 1.

Similar as observed for the correlations of τ_{ij}^d), $\mathcal{P}$ and k_{sgs} become less correlated with the increase in rotation. The effects of rotation on an initially homogeneous isotropic flow is to suppress the enstrophy production. In the end, this reduces the energy dissipation rate, which is more relevant at the small scales. Therefore, the low correlation levels for $\mathcal{P}$ found in Tab. 1 for the rotating cases suggest that none of these models is able to capture the effects of rotation on the SGS dynamics. This statement is based on the fact that $\mathcal{P}$ is the one responsible for transferring energy from the resolved to the subgrid-scales, where it is later dissipated.

A more detailed comparison that provides information regarding the distribution of $\mathcal{P}$ is obtained from its p.d.f.,

which is presented in Fig. 2. The DNS data for the three different flow cases show that the p.d.f. is asymmetric and includes positive and negative values. Although on average $\mathcal{P}$ is positive, the negative values of $\mathcal{P}$ imply a local energy transfer from the subgrid to the resolved scales — energy backscatter. Note, however, that none of the models can reproduce the local backscatter, as their formulation *per se* do not allow negative values.

The effects of rotation are evident by comparing Fig. 2a and Fig. 2c, for instance. Overall, we see that rotation favors an asymmetric p.d.f. The asymmetry is imprinted in the skewness of $\mathcal{P}$, for which we find a value of 3.841 in the isotropic case, and 4.845 and 10.517 for the weak and strong rotation cases, respectively. The p.d.f. also develops heavier tails with increasing rotation rate, indicating that extreme events, although unlikely, can occur. This is measured by the flatness of $\mathcal{P}$, which varies from 29.867 for the isotropic case to 59.951 (weak) and 598.288 (strong) for the cases with rotation. As comparison, the skewness and the flatness of the p.d.f. of $\mathcal{P}$ with the DEA are, respectively, 4.390 and 37.637 (isotropic), 4.475 and 39.690 (weak rotation) and 9.331 and 170.720 (strong rotation). Figure 2 also clarifies the difference in performance between models. In the isotropic case, for instance, the positive values of $\mathcal{P}$ are well captured by both the EA models, in contrast with the results for the DSM. This can be intriguing at first because we saw from Tab. 1 that the correlation of $\mathcal{P}$ for the DSM and the DEA are of the same magnitude. However, it is important to note that correlation coefficients are unaffected by scaling any of the fields with a positive constant. With rotation (Fig. 2b and Fig. 2c), the p.d.f. of $\mathcal{P}$ is poorly captured and the DEA outperforms the SEA. Interestingly, for the isotropic case the situation is reverse and a better match for the p.d.f. is obtained with the SEA.

PRESSURE-STRAIN MODELS

Hereafter we let the DSM aside and focus on the two EA models only, i.e., SEA and DEA. Through correlations, we investigate the performance of three different pressure-strain models and the local equilibrium assumption, i.e., $\mathcal{P}/\varepsilon = 1$. The correlation coefficient for the dif-
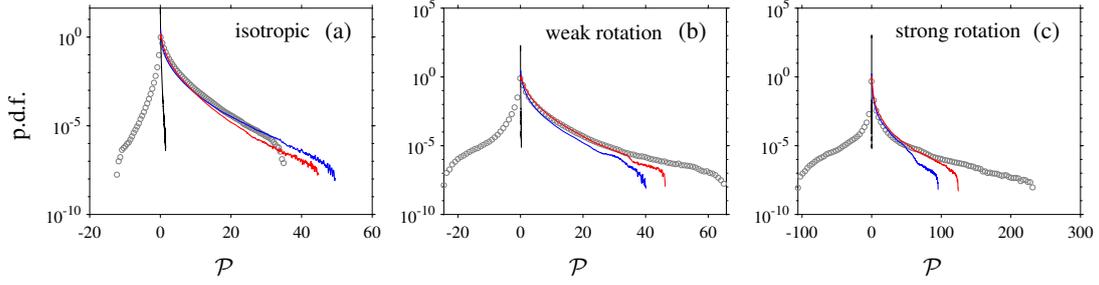
Figure 2: Probability density function of the production term responsible for the inter-scale energy flux for case isotropic (a), weak rotation (b) and strong rotation (c). (○) represents the filtered DNS data, whereas the different line types correspond to different LES models: DSM (—), SEA (—) and DEA (—).

ferent pressure-strain models are shown in Fig. 3 for all the three flow cases. In Fig. 3a, isotropic turbulence, the correlation coefficient of all the components of Π_{ij} are indistinguishable for the linear models (LRR-QI and LRR-IP). The non-linear model (SSG) also behaves similarly and a correlation coefficient of roughly 0.5 is found for all the models. Regardless of the model, Figs. 3b and 3c show that rotation leads to a lower degree of correlation. Nevertheless, the loss in correlation occurs gradually and a correlation of 0.3 is still found for the weak rotating case. For the strong rotating case, Fig. 3c shows that the correlation of the components of the pressure-strain field becomes negative or even uncorrelated. The largest deviation from the isotropic case is observed for Π_{12}. In general, however, we do not observe substantial differences in the correlation levels between the linear and the non-linear models. In Fig. 3, the trend of the SSG model is similar to both LRR models.
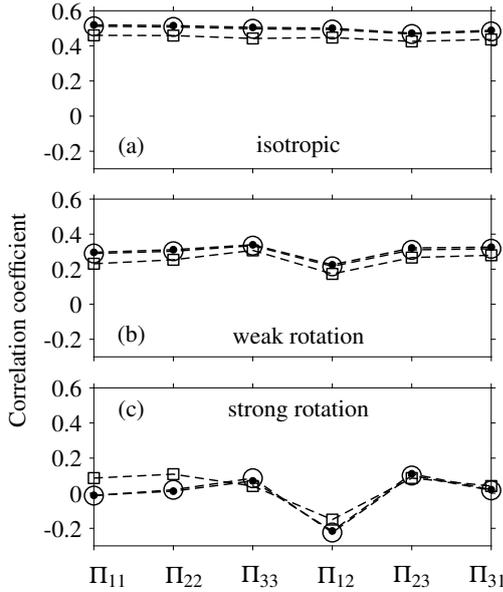
As for the rapid and slow pressure-strain terms, i.e,

Π_{ij}^{rapid} and Π_{ij}^{slow}, the correlation coefficients are shown in Fig. 4 for the isotropic and the strong rotating case. Results for the isotropic case indicate that the rapid term is better correlated to the actual DNS data than the slow term, and that the correlation coefficients for Π_{ij}^{rapid} are twice as large as for Π_{ij}^{slow}. Effects of rotation are also more pronounced in the rapid terms. For all the pressure-strain models, we observe that the correlation coefficients approaches zero and the different components of Π_{ij}^{rapid} behave similarly to Π_{ij} in Fig. 3c. Therefore, we attribute the poor performance of the pressure-strain models observed in Fig. 3 mainly to the modeling of Π_{ij}^{rapid}. Again, the performance of the LRR and SSG models are similar.

Figure 3: Correlation coefficients of the modeled and actual pressure-strain tensor: LRR-QI (-⊖-), LRR-IP (-•-) and SSG (-▫-). Different panels corresponds to the different flow cases: isotropic (a), weak rotation (b) and strong rotation (c).
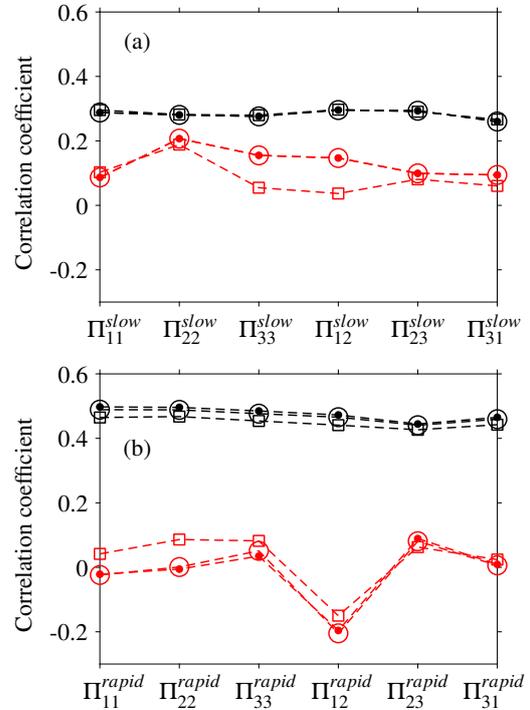

Figure 4: Correlation coefficients for the slow (a) and rapid (b) parts of the pressure-strain term. Only two cases are considered: isotropic (- - -) and strong rotation (- - -). Symbols denote distinct pressure-strain models: LRR-IP (•), LRR-QI (○) and SSG (▫).
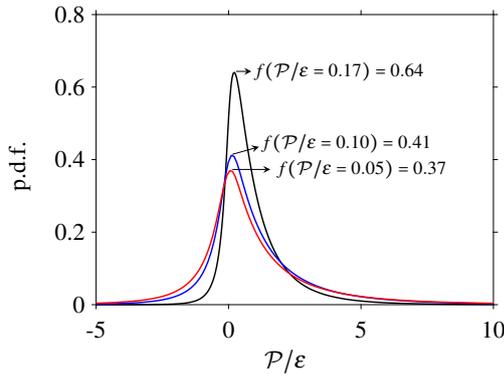
Figure 5: Probability density function for $\mathcal{P}/\varepsilon$: isotropic (—), weak rotation (—) and strong rotation (—).

LOCAL EQUILIBRIUM ASSUMPTION

Now we turn our attention to the local equilibrium assumption between SGS energy production and dissipation. Figure 5 presents the p.d.f. of $\mathcal{P}/\varepsilon$ in order to test the validity of the assumption. We make two main observations. First, as rotation increases, the p.d.f. develops heavier tails similar to Fig. 2. Second, the ratio $\mathcal{P}/\varepsilon$ is distributed over a broad range of values with mean, obtained after numerical integration of the p.d.f., equals 0.91 (isotropic), 1.08 (weak) and 0.96 (strong).

The practice to set $\mathcal{P}/\varepsilon = 1$ avoids the non-linearity on the l.h.s. of Eq. (3). In Marstorp *et al.* (2009), the authors justify this choice based on a energy budget where $\langle \mathcal{P} \rangle = \langle \varepsilon \rangle$. (The symbol $\langle \cdot \rangle$ represents box-averaged quantities). While this is one possibility, another choice is to fix $\mathcal{P}/\varepsilon$ in Eq. (3) to its mean value. Nevertheless, we must bear in mind that $\langle \mathcal{P}/\varepsilon \rangle$ is essentially different from $\langle \mathcal{P} \rangle / \langle \varepsilon \rangle$. Equation (3) is assumed to hold locally. Therefore, if calibrated to a constant, the approximation should be based on $\mathcal{P}/\varepsilon$ and not on $\mathcal{P}$ and ε individually. For example, the maximum likelihood value, i.e., the peak of the p.d.f. of $\mathcal{P}/\varepsilon$, could be an estimate. However, this requires prior knowledge of the p.d.f. of $\mathcal{P}/\varepsilon$, which depends on the flow type. For instance, in Fig. 5, the value of maximum likelihood reduces monotonically with increasing rotation from 0.17 (isotropic) to 0.1 (weak rotation) and 0.05 (strong rotation).

CONCLUSIONS

We have evaluated the overall performance of EASSMS and the validity of their main ingredients by means of an *a priori* analysis using data from DNS. We observed that the correlation coefficients of the actual and modeled τ_{ij} are improved for both EA models with respect to the DSM. Overall, a better match is found with the DEA. The EA models also show better correlations for $\mathcal{P}$, and it was evident that they can reproduce the spatial distribution of $\mathcal{P}$ significantly better than the DSM. In order to investigate the underlying assumptions of the EA models, two building blocks of these models are assessed: the modeling of Π_{ij} and the local equilibrium assumption. Regarding the modeling of Π_{ij}, we showed that the LRR-IP, the LRR-QI and the SSG models record similar levels of correlation regardless of the strength of rotation. Nevertheless, a deterioration of the correlation level was observed for all three models for increasing rotation rate. We also further split the contributions of the pressure-strain correlation in its rapid and slow parts. We saw that the main cause for a loss in correlation stems from the modeling of Π_{ij}^{rapid}. With respect to the local equilibrium assumption, the p.d.f. of $\mathcal{P}/\varepsilon$ presents a clear evidence that $\mathcal{P}/\varepsilon$ is distributed over a broad range of values. Moreover, the properties of the p.d.f changes with rotation, indicating that assuming $\mathcal{P}/\varepsilon = 1$ can be only viewed as a simplification that offers simplicity in the derivation of explicit relations for τ_{ij}.

REFERENCES

Alvelius, K. 1999 Random forcing of three-dimensional homogeneous turbulence. *Physics of Fluids* **11**, 1880–1889.

Launder, B. E., Reece, G. J. & Rodi, W. 1975 Progress in the development of a Reynolds-stress turbulence closure. *Journal of Fluid Mechanics* **68**, 537–566.

Lilly, D. K. 1992 A proposed modification of the Germano subgridscale closure method. *Physics of Fluids A: Fluid Dynamics* **4** (3), 633–635.

Lumley, J. L. 1979 Computational modeling of turbulent flows. *Advances in Applied Mechanics* **18**, 123–176.

Marstorp, L., Brethouwer, G., Grundestam, O. & Johansson, A. V. 2009 Explicit algebraic subgrid stress models with application to rotating channel flow. *Journal of Fluid Mechanics* **639**, 403–432.

Pekurovsky, Dmitry 2012 P3DFFT: A Framework for Parallel Computations of Fourier Transforms in Three Dimensions. *SIAM Journal on Scientific Computing* **34** (4), C192–C209.

Pestana, T. & Hickel, S. 2019 Regime transition in the energy cascade of rotating turbulence. *Physical Review E* **99** (5), 053103.

Pope, S. B. 1975 A more general effective-viscosity hypothesis. *Journal of Fluid Mechanics* **72**, 331–340.

Rodi, W. 1972 *The prediction of free turbulent boundary layers by use of a two-equation model of turbulence*. University of London.

Rogallo, R. S. 1977 An ILLIAC program for the numerical simulation of homogeneous incompressible turbulence. *NASA Technical Memo* **73**, 203.

Speziale, C. G., Gatski, T. B. & Sarkar, S. 1992 On testing models for the pressure–strain correlation of turbulence using direct simulations. *Physics of Fluids A: Fluid Dynamics* **4**, 2887–2899.

Speziale, C. G., Sarkar, S. & Gatski, T. B. 1991 Modelling the pressure–strain correlation of turbulence: an invariant dynamical systems approach. *Journal of Fluid Mechanics* **227**, 245–272.

Townsend, A. A. 1954 The uniform distortion of homogeneous turbulence. *The Quarterly Journal of Mechanics and Applied Mathematics* **7**, 104–127.

Zeman, O. 1994 A note on the spectra and decay of rotating homogeneous turbulence. *Physics of Fluids* **6**, 3221–3223.